



# Role of Martensite Structural Characteristics on Corrosion Features in Ni-Advanced Dual-Phase Low-Alloy Steels

Chao Hai<sup>1</sup> · Xuequn Cheng<sup>1</sup> · Cuiwei Du<sup>1</sup> · Xiaogang Li<sup>1</sup>

Received: 24 March 2020 / Revised: 28 May 2020 / Accepted: 27 July 2020 / Published online: 22 October 2020  
© The Chinese Society for Metals (CSM) and Springer-Verlag GmbH Germany, part of Springer Nature 2020

## Abstract

The relationship between the corrosion resistance and martensite structure of Ni-advanced dual-phase weathering steel was studied using transmission electron microscopy, scanning electron microscopy, electrochemical analysis, and atomic force microscopy. The investigations indicate that the final microstructure of the dual-phase weathering steel was composed of a large amount of low-carbon lath martensite distributed in the ferrite matrix. The potential of the martensite phase is higher than that of ferrite, which acts as a microcathode. As the martensite volume fraction in the Ni-advanced dual-phase weathering steel increased, the corrosion rate increased owing to the greater galvanic couple formed between the ferrite and martensite from the increasing ratio of the cathode area to the anode area. In addition, this work provides a method to obtain advanced weathering steel with improved mechanical properties and corrosion resistance.

**Keywords** Weathering steel · Corrosion · Martensite · Dual phase · Galvanic couple

## 1 Introduction

Weathering steels (WSs) are classified as low-carbon steels and are mainly alloyed with Cu, P, Cr, and Ni in a total proportion of less than 3–5 wt% [1–4]. Ni is specifically introduced into WS to develop Ni-advanced WSs, which are widely used in coastal structures [5–9]. At present, research on the atmospheric corrosion resistance of WSs has focused on the effect of alloying elements and grain size [2, 5, 7, 10]. Cheng et al. [5] investigated the effect of Ni on the corrosion resistance of WSs in acidic atmospheres. They found that 3.5 wt% is the optimum Ni concentration in WSs to enhance their atmospheric corrosion resistance. However, the effect of the microstructure on the corrosion resistance is still unclear.

Dual-phase (DP) steels have attracted considerable research [11–16] for their interesting combination of high strength, good formability, continuous yielding, and low yield stress to tensile strength ratio, which have broad

application prospects in the automotive industry. Lan et al. [13] developed DP steel through intercritical annealing of cold-rolled martensite. In this case, the fine ferrite grain size as well as uniform distribution of the martensite enhanced the work hardening, showing an improved strength-ductility balance. DP steels are generally produced by an intercritical heat treatment, and their microstructures mainly consist of hard martensite particles dispersed in a soft ductile ferrite matrix [17, 18]. However, the corrosion resistance of devices is crucial to meet the requirements for long-term service of materials. Therefore, heat treatments can be applied to obtain DP WS with good atmospheric corrosion resistance and mechanical properties [19, 20].

Some studies have recently been conducted on the corrosion resistance of DP steels [4, 12, 21, 22]. Bhagavathi et al. [4] developed a plain low-carbon DP steel and found that it had better corrosion resistance than subcritically heat-treated ferrite-pearlite steel. Keleştemur and Yıldız [12] studied the corrosion behavior of six types of DP steels with different martensite morphology and concentrations. Based on these findings, the amount and distribution of martensite considerably influenced the corrosion resistance. With increasing martensite content in the steel, the corrosion resistance of DP steels gradually deteriorated. Sarkar et al. [22] performed an investigation to measure the galvanostatic corrosion behavior of five DP steel specimens. Their findings

Available online at <https://link.springer.com/journal/40195>

✉ Xuequn Cheng  
chengxuequn@ustb.edu.cn

<sup>1</sup> Institute of Advanced Materials and Technology, University of Science and Technology Beijing, Beijing 100083, China

show that a larger martensite content and a higher degree of structural refinement will increase the corrosion rate. Allam and Abbas [20] investigated the formability and corrosion behavior of DP WSs developed by an intercritical annealing treatment. The results indicated that the presence of martensite increased the corrosion rate of DP WSs during the initial corrosion process, but it could accelerate the nucleation of the protective layer.

Although considerable research has been conducted, further investigation is required on the effect of various morphologies and different volume fractions of ferrite and martensite in DP steels on corrosion behavior. The effect of different volume fractions of ferrite and martensite on the corrosion behavior was the focus of this research.

## 2 Experimental

### 2.1 Materials Preparation and Heat Treatment

The WSs were self-developed and melted in a 20 kg vacuum induction furnace. The chemical composition of the steel was C-0.059%, Si-0.087%, Mn-1.23%, P-0.006%, S-0.008%, and Ni-3.21%.

After forging and rolling, the specimens were normalized to eliminate the influence of temperature unevenness on the structure of the sample during rolling and then heated to

880 °C before quenching. All the specimens were sub-heated at 880 °C for 0.5 h and then air cooled, which is a common process used to develop DP steels. Critical temperatures  $A_{c1}$  and  $A_{c3}$  were calculated to be 658 and 848 °C, respectively. The microstructure was achieved by annealing at different intercritical temperatures for 30 min and cooling in oil. Figure 1 shows a schematic representation of the applied thermal cycles. In addition, normalized and quenched WSs were selected as control samples.

The microstructures of the steels were observed using a Zeiss optical microscope after being polished with 3000 grit sandpaper and etched. The martensite volume fractions (MVs) in the experimental steel were measured using self-contained analysis software. Furthermore, the microhardness of four specimens was measured using a microhardness tester.

### 2.2 Corrosion Behavior

Specimens prepared for the indoor simulated corrosion test were cut to 50 mm × 25 mm × 5 mm. The parameters for the indoor simulated cycle corrosion test are listed in Table 1. All specimens were ground with 240–800 grit sandpaper and cleaned with deionized water, acetone, and absolute ethyl alcohol. The samples were weighed after drying with cold wind and recorded as *W<sub>0</sub>* (average values

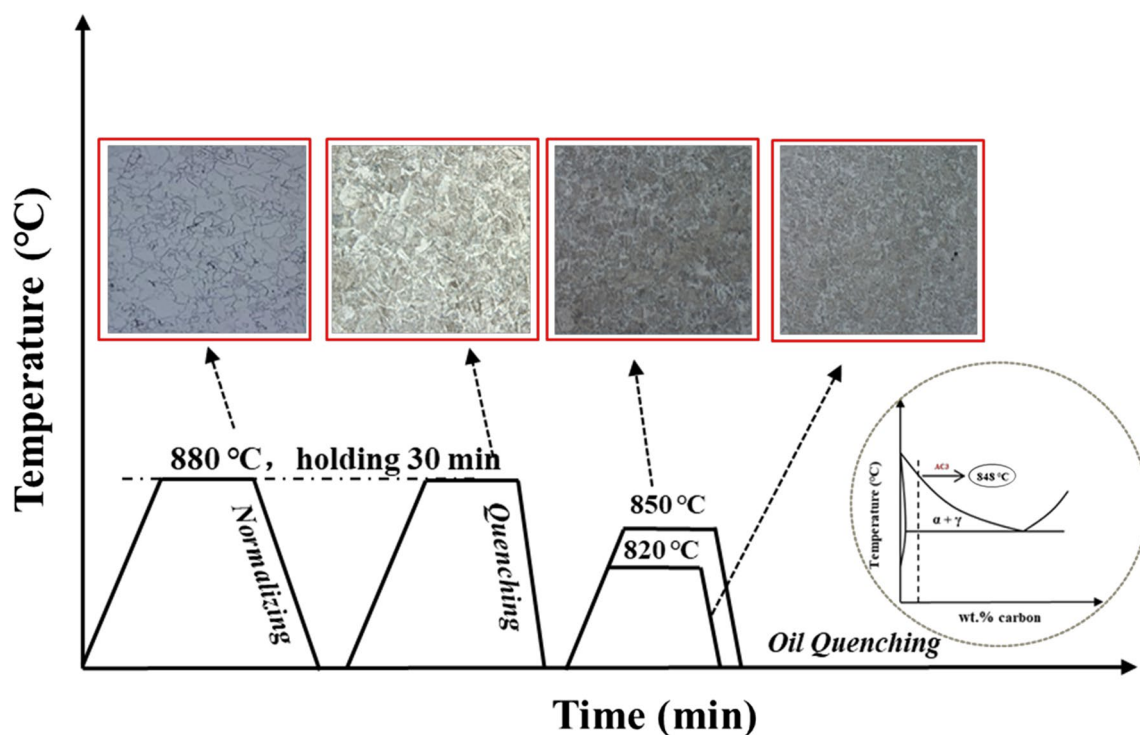


Fig. 1 Schematic representation of the applied thermal cycles

**Table 1** Parameters for the cycle corrosion test

Cycle time (min)	Immersion time (min)	Drying time (min)	Solution temperature (°C)	Sample surface temperature (°C)	Relative humidity	Test period (h)
60	15	45	40	40 ± 2	40 ± 2	72

of weighing three times), with a precision of 0.0001 g. Then, the corrosion rate ( $R$ , mm/a) of the exposed steels was calculated as follows:

$$R = \frac{(W_0 - W_t) \times 10^{-2}}{S\rho t}, \quad (1)$$

where  $(w_0 - w_t)$  represents the weight loss of each parallel sample after exposure for one year, g;  $S$  represents the exposed area of sample, cm<sup>2</sup>;  $\rho$  represents the density of the WS, 7.8 g cm<sup>-3</sup>; and  $t$  is the exposure time, a.

Electrochemical impedance spectroscopy (EIS) measurements were performed using a P4000 electrochemical workstation in a conventional three-electrode system. The test steels were used as the working electrodes with an exposed area of 1 cm<sup>2</sup>, and a Pt plate and a saturated calomel electrode (SCE) were used as the counter electrode and reference electrode, respectively. The test solution was 3.5% NaCl without pH adjustment. After the open-circuit potential reached a steady state, EIS was performed with an amplitude of 10 mV and a frequency ranging from 10<sup>6</sup> to 10<sup>-2</sup> Hz.

The immersion test was conducted in a 3.5% NaCl solution with a pH of 5.6. According to GB/T 19746-2005, the rust-removing solution was selected to clean the corrosion products on the surface of the samples. The rust remover contained 500 mL of hydrochloric acid, 500 mL of deionized water, and 3.5 g of hexamethylenetetramine. The surface and cross-sectional morphologies of the rust layer of the carbon steel samples were observed by scanning electron microscopy (SEM, Quanta 250). In addition, the chemical compositions of the corrosion products and the elemental distribution on the cross section of the product film were analyzed by energy-dispersive X-ray spectroscopy (EDS).

## 2.3 AFM Measurements

Atomic force microscopy (AFM) was used to measure the potential difference and morphology of the microstructures. The experiment was performed with a Bruker MultiMode 8 atomic force microscope system at room temperature. A PFQNE-A1 probe was used for the measurements. In the experiment, the surface topography and potential distribution were measured synchronously by AC one-way measurements with scanning at 0.5 Hz.

## 3 Results and Discussion

### 3.1 Microstructure Characterization

The typical microstructure of the hot-rolled WS is shown in Fig. 1. The initial microstructure of the normalized steel was irregular massive ferrite (bright region) with sporadic pearlite (dark region) distributed at the grain boundaries. The micrographs of the specimens after treatment at different critical temperatures are shown in Fig. 1. This microstructure mainly consisted of ferrite and lath martensite, which can be clearly distinguished in the TEM image. The MVF varied with the holding temperature before quenching during heat treatment. With increasing temperature, the MVF increased. The annealing temperature of 820 °C yielded the lowest MVF (59.02%). Because the holding time (30 min) was sufficient for the complete dissolution of pearlite and austenite growth in ferrite, relatively larger austenite grains could be formed at higher temperatures.

Table 2 lists the hardness of the DP WSs. RA is the abbreviation of residual austenite. With increasing MVF, the hardness of the DP WSs also increased. In this paper, “xxx% martensite” is used to identify the specimens that contained various amounts of martensite under different temperatures.

**Table 2** Hardness of the DP WSs formed with different heat treatments

Heat temp.	Microstructure	MVF (%)	Hardness (HRC)
880 °C for 30 min, then normalizing	Ferrite + pearlite	6.7 (the volume fraction of pearlite)	17.8
820 °C for 30 min, then oil quenching	Ferrite + lath Martensite + RA	59.02	22.8
850 °C for 30 min, then oil quenching	Ferrite + lath Martensite + RA	74.11	27.5
880 °C for 30 min, then oil quenching	Martensite + RA	≈ 100	32.5

Allam and Abbas [20] have reported that carbon diffusivity, mobility of the moving  $\gamma/\alpha$  interface, and chemical driving force for austenite formation increase as the intercritical annealing temperature increases. Higher temperatures then lead to the formation of larger amounts of austenite, resulting in the formation of larger amounts of martensite after quenching [17]. Because increasing the temperature reduces the carbon solubility in austenite, various microstructures containing martensite and ferrite formed after quenching.

TEM images of the DP WSs formed with different heat treatments are shown in Fig. 2. Martensite laths and ferrite can be distinguished by their morphological characteristics. When the quenching temperature was 850 °C, the average lath spacing of the martensite was 450 nm (shown in Fig. 2b), while it was 250 nm for the others (shown in Fig. 2a). Additionally, Fig. 2c and d presents more uniform fine martensitic lath bundles, and some laths are divided into substructures by laths with abnormal growth directions. The fine microstructure may enhance the corrosion resistance of WS if the negative influence of grain growth at high temperatures is ignored (shown in Fig. 1). Furthermore, it can be observed in Fig. 2 that there are numerous dislocations in the ferrite and some dislocations accumulate to form dislocation clusters. With increasing temperature, the dislocation density in ferrite increases, which may affect the corrosion behavior of WSs.

### 3.2 AFM Analysis

The surface morphology and surface potential maps of the three DP WSs were obtained using AFM. In general, the surface potential is regarded as a criterion for measuring the relative quality of materials [23, 24]. Figure 3 shows the results of the AFM analysis of the WS with 59.02% martensite. It can be seen from the surface morphology shown in Fig. 3a that WS 1 was composed of dual phases (ferrite and martensite). Figure 3b shows that potential differences existed between the martensite laths, with an average value of 23 mV. In addition, potential differences were also observed between the ferrite and martensite in the WSs. As shown in Fig. 3d, the average potential of the martensite was approximately 17 mV higher than that of the ferrite, and the potential at the grain boundary of the ferrite phase was also higher than that in the ferrite crystal. It has been reported that some carbon and other elements diffuse from martensite and then migrate and accumulate at the grain boundary during the DP heat treatment, which improves the energy at the grain boundary. Compared with the results measured by Liu et al. [25], the potential difference between different structures of the two phases was much smaller than that between the rare-earth modified inclusions and the steel matrix. Wei et al. [26] also researched the early corrosion development

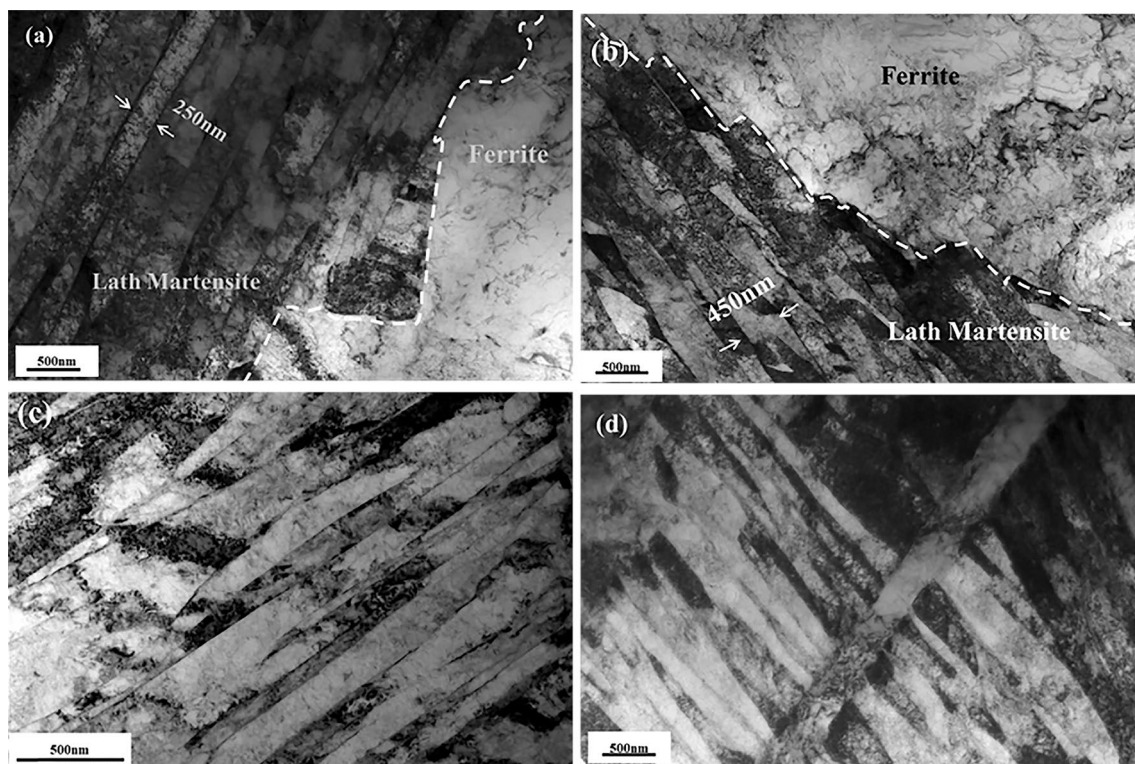


**Fig. 2** TEM images of the DP WSs treated with different heat treatments: **a** 59.02% martensite, **b** 74.11% martensite, **c**, **d** 100% martensite

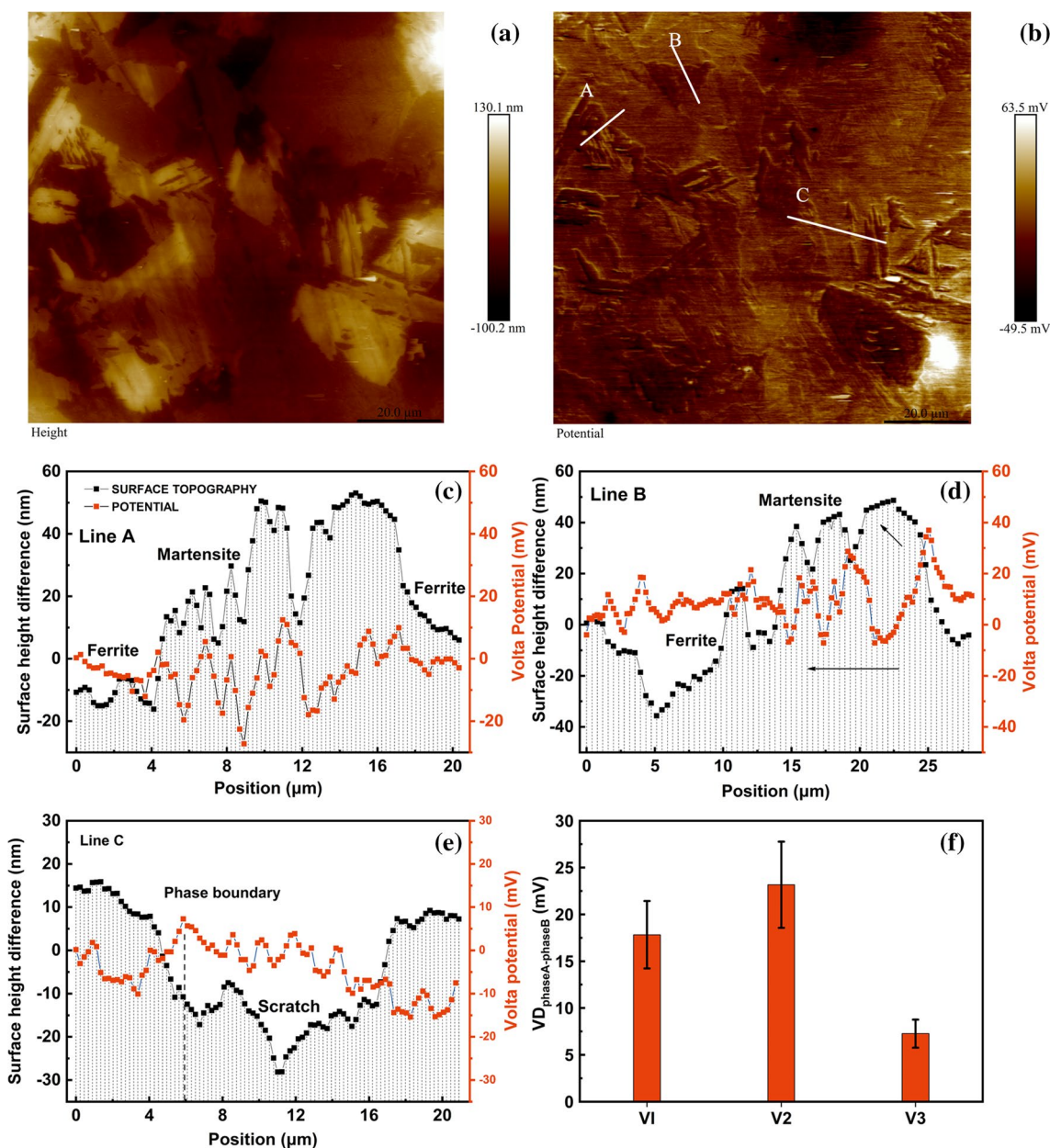


**Fig. 3** AFM results of the WS with 59.02% martensite: **a** surface topography, **b** surface potential distribution map, **c** analysis results of line A, **d** analysis results of line B, **e** analysis results of line C, **f** statistical results of the potential differences between different phases (V1 is the average potential difference between martensite and ferrite, V2 is the potential difference between the slats, and V3 is the potential difference between the ferrite grain boundary and the ferrite)

process of high-strength, low-carbon, and low-alloy steels by in situ AFM and scanning vibration electrode technology (SVET). It was expounded that the local corrosion of low-alloy steels caused by inclusions developed into uniform corrosion, which was controlled by the galvanic action caused by the potential difference between different phases in the electrode reaction system. Based on previous results [25, 27, 28], corrosion preferentially originates from defects, such as inclusions and high-density

dislocation regions. From the results of this experiment, it can be seen that both the ferrite and martensite phases are prone to local corrosion with different intensity levels. The corrosion resistance of DP steels is governed by the local corrosion of each individual phase and the galvanic corrosion between them. However, considering the phase distribution of the two phases in steel and the large ratio of the cathode area to the anode area, the galvanic couple may play an important role in the development of corrosion.

Figure 4 shows the AFM results of the WS with almost 100% martensite. The microstructure consists of lath martensite, and the lath spacing is clearly observed. Figure 4b and c shows the surface potential distribution lines in two positions, which demonstrate the internal potential difference of martensite with different grain orientations. Therefore, the uneven distribution of potential leads to a difference in the sensitivity of different martensite grains to corrosion. An area with high potential is used as the cathode phase to accelerate the corrosion of the anode phase with low potential.

### 3.3 Electrochemical Behavior

Figure 5 shows the polarization curves of the four WSs. As can be seen from the figure, the steels exhibited similar electrochemical behavior. A comparison of the polarization curves of the four WSs shows that the corrosion current density is almost the same, but the corrosion potential marginally decreased from  $-0.64$  to  $-0.67$   $V_{SCE}$  as the quenching temperature increased from 820 to 880 °C, respectively,

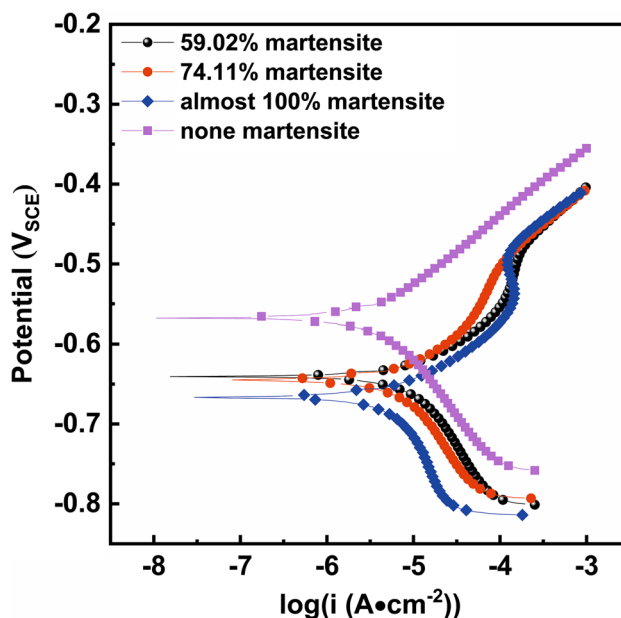


Fig. 5 Polarization curves of WSs after different heat treatments

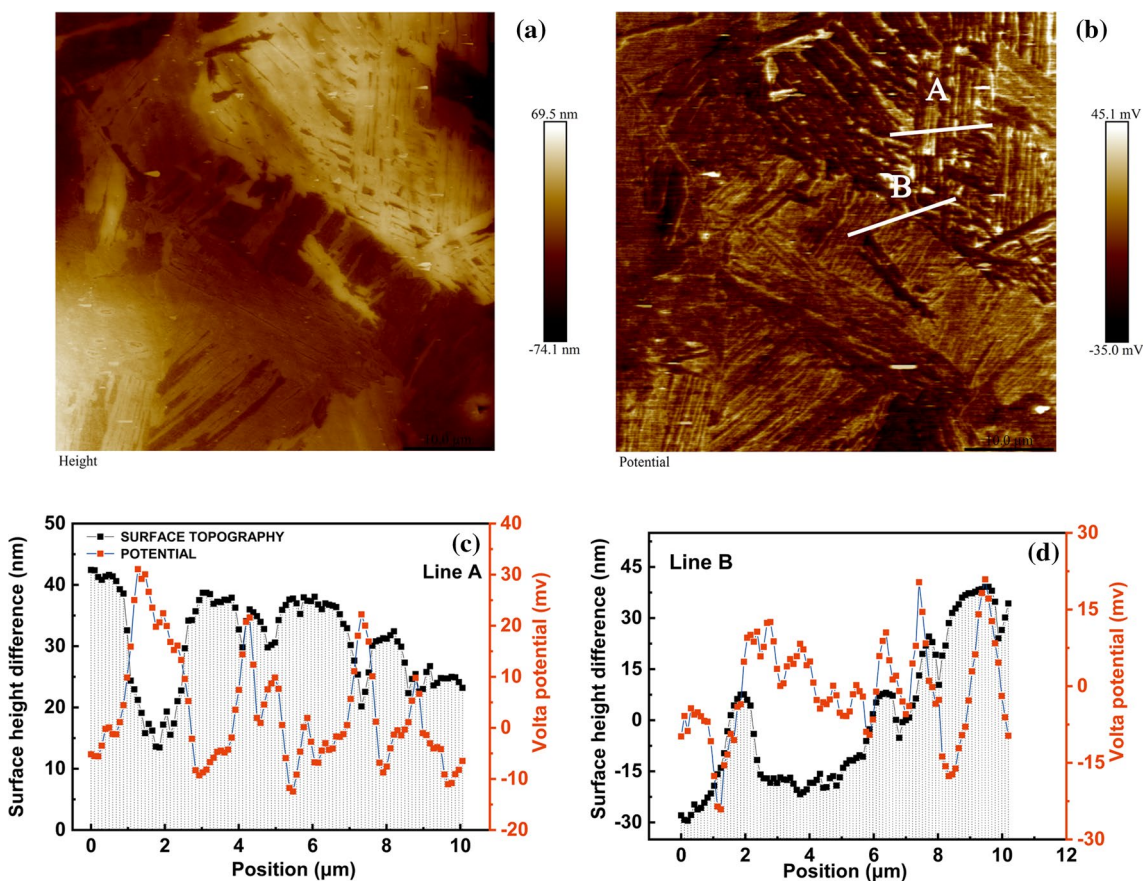


Fig. 4 AFM results of the WS with almost 100% martensite: a surface topography, b surface potential distribution map, c analysis results of line A, d analysis results of line B

which indicates better resistance to corrosion was achieved after quenching at lower temperatures.

EIS measurements are typically taken to investigate the corrosion mechanism of corroded steel [29–33]. Figure 6 shows the EIS results for the WSs in a 3.5% NaCl solution at room temperature. These curves contain a single capacitance arc, indicating that the corrosion resistance of the steel decreased with increasing temperature. Accordingly, the EIS curves can be simulated using the equivalent electric circuit of  $R(QR)$ , where  $R_s$  is the solution resistance,  $C_{dl}$  represents the capacitance of the double electrode layer, and  $R_{ct}$  signifies the charge transfer resistance. The fitted results are listed in Table 3; they indicate that normalized steel provides better corrosion resistance in the early stage of corrosion compared with other WSs. Considering the microstructure of the samples, the numerous micro-couples between martensite and ferrite could accelerate the corrosion rate of samples in the early stage in a 3.5% NaCl solution.

After polarization testing, the surface topography was observed by SEM. Figure 7a shows the corroded surface of normalized WS. A large number of pits and grain boundaries could be observed over the entire area. During the process of polarization, the ferrite grain dissolved, and the cementite remained, gathering around the grain boundary. Figure 7b–d shows the corroded surfaces of the DP WS samples. The corrosion pits are shallow in size in the WS treated at 820 °C.

Numerous widespread small pits could also be observed on the surface, unlike in normalized WS. It can be seen in the partial enlarged drawing that the areas (where the origin arrow is pointing) are the high potential regions. Therefore, initially during corrosion, the high-potential region worked as the cathode and the nearby area was first corroded and fully removed; thus, pits were formed. Comparing all the figures, the severity of pitting is least for the WS sample treated

**Table 3** Electrochemical impedance spectrum fitting data

Heat temp.	$R_s$ ( $\Omega \text{ cm}^2$ )	Cdl	$R_{ct}$ ( $\Omega \text{ cm}^2$ )
None Martensite	6.17	$6.985 \times 10^{-4}$	1877
59.02% martensite	5.75	$9.246 \times 10^{-4}$	1486
74.11% martensite	6.45	$9.551 \times 10^{-4}$	1154
100% martensite	6.77	$7.752 \times 10^{-4}$	1228

at 820 °C. Large pits can be observed in both Fig. 4c and d, indicating that serious corrosion occurred in two types of steel during polarization.

The corrosion rates for the normalized steel and DP WSs were calculated according to Eq. (1), and the results are summarized in Fig. 8. The corrosion rates increased with increasing MVF in the WSs. The amount of martensite is an impact factor for the corrosion rate of DP WSs. The microstructures obtained at lower quenching temperatures (820 °C) were composed of fine lath martensite and ferrite.

Figure 9 shows the surface morphology of the WSs after immersion for 30 d in a 3.5% NaCl solution. As shown in Fig. 9, there were obvious differences among the corrosion morphologies. After immersion for 30 d, the grains in the normalized steel dissolved, and the cementite remained, which gathered around the grain boundary. During the corrosion process, the cementite around the grain boundaries (as the cathode) promoted the dissolution of the ferrite, which was divided into the anode phase. The corrosion morphology of DP WSs was similar. Both the ferrite and martensite phases were prone to local corrosion. Part of the ferrite was corroded and detached; therefore, a unique corrosion morphology appeared. The ferrite inside and around the martensite was corroded, and the corrosion pit around the martensite was deep and serious, as shown in Fig. 9d.

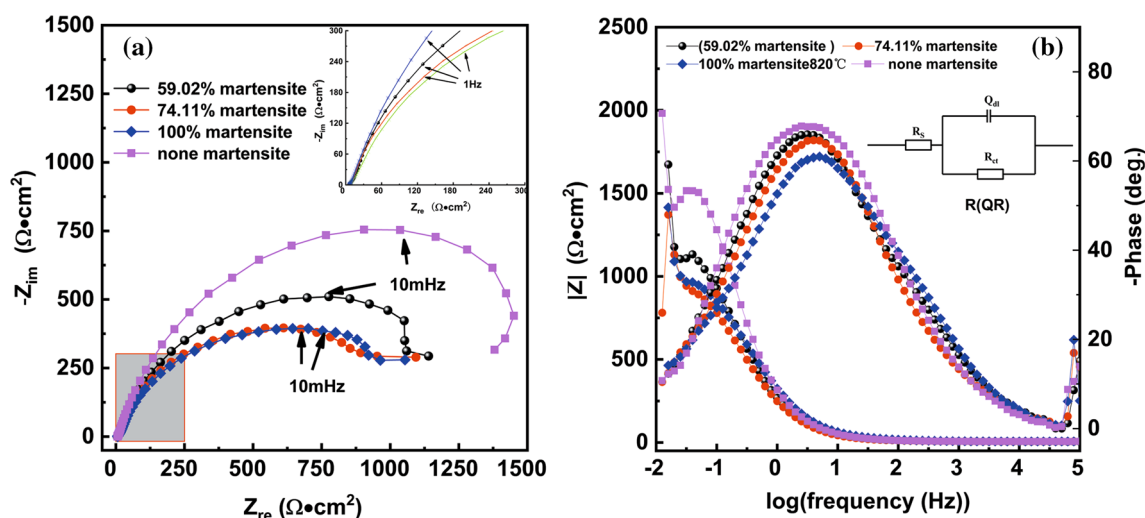


**Fig. 6** EIS results of the DP WSs: **a** Nyquist, **b** Bode plots

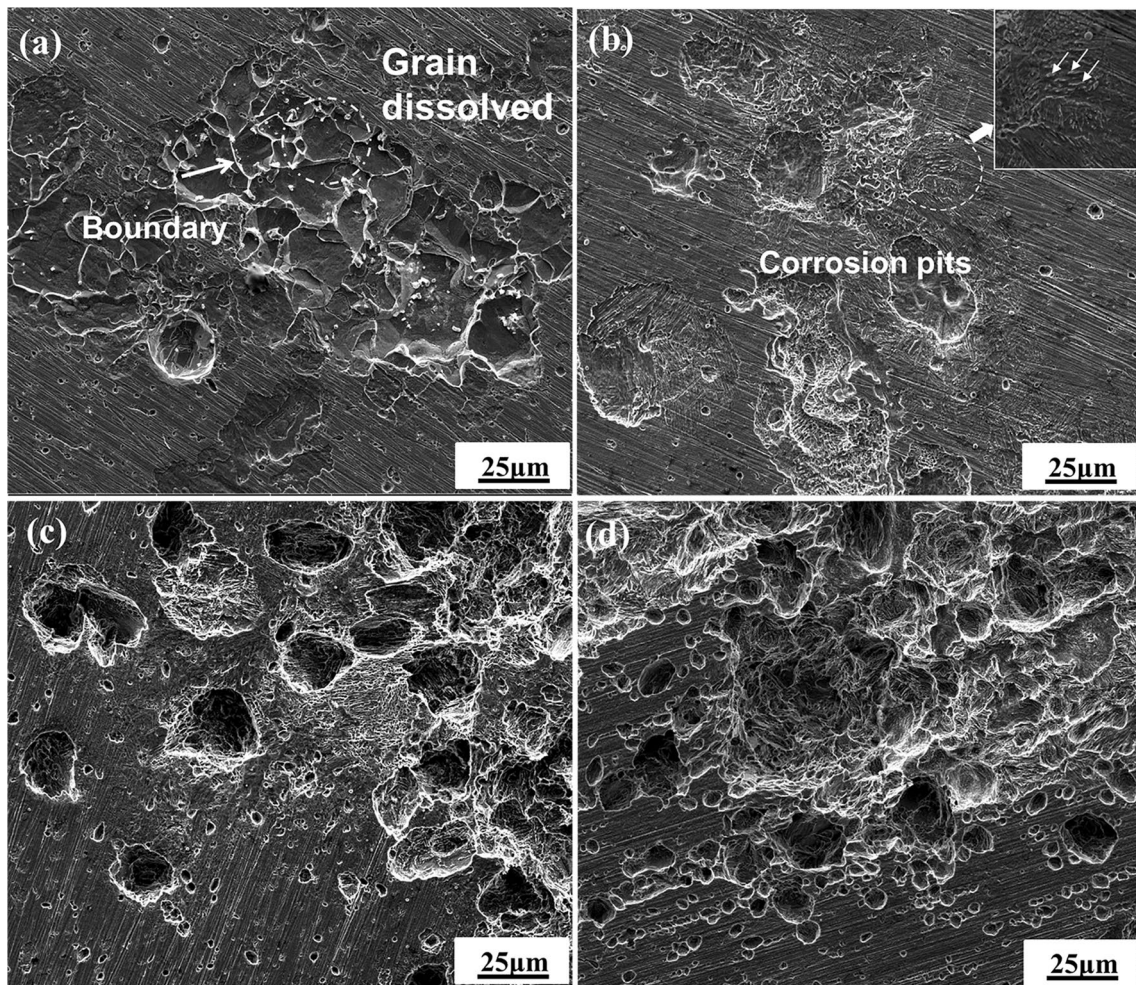


Fig. 7 SEM micrographs of corroded samples after polarization testing: a none martensite, b 59.02% martensite, c 74.11% martensite, d 100% martensite

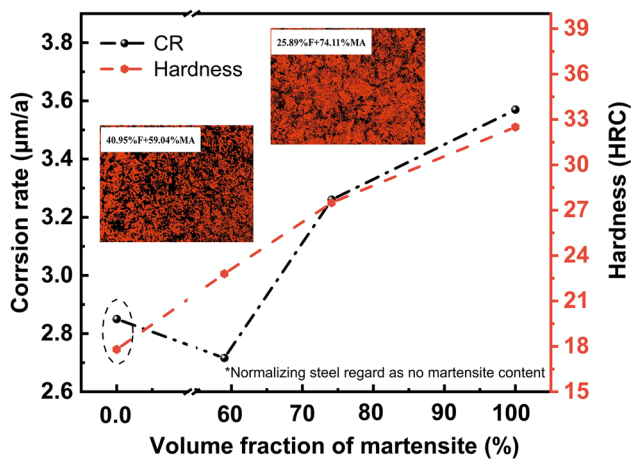


Fig. 8 Corrosion rate of the treated specimens

A detailed investigation was performed using micro-Raman spectroscopy to study the phase compositions of the product, and the results are displayed in Fig. 10. As shown in Fig. 10, the product films on the four WSs were mainly composed of lepidocrocite. Negligible difference in composition was observed between the four curves. This can be explained by two factors. One is that, after a short immersion test, the WSs have similar corrosion behaviors; thus, the difference in composition is not noticeable. The other reason is that, before the steel forms a protective rust, the microstructure of the steel may have a weaker influence on corrosion.

### 3.4 Discussion

Many studies [4, 19, 20, 29] have shown that steels present advanced corrosion resistance after treatment at an appropriate intercritical annealing temperature. The present investigation concerns the study of WSs treated by near-critical annealing treatments. The results showed that the



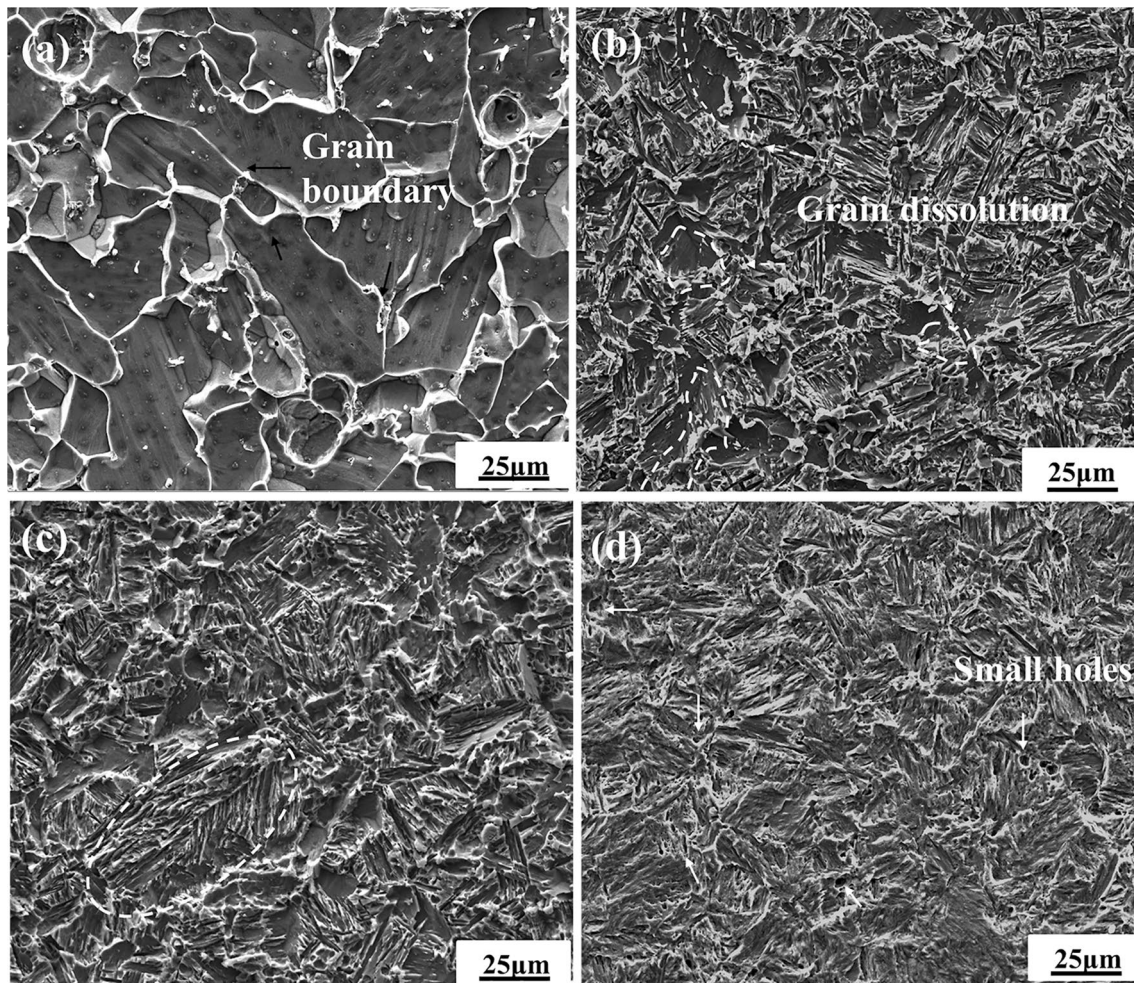


**Fig. 9** Surface morphologies of WSs after immersion for 30 d in a 3.5% NaCl solution: **a** none martensite, **b** 59.02% martensite, **c** 74.11% martensite, **d** 100% martensite

microstructure of WS consisted primarily of martensite distributed in a ferrite matrix. At the lowest intercritical annealing temperature (820 °C), the martensite showed an interconnected morphology, and its average lath spacing was the smallest of the DP WSs (250 nm). The potential difference between the martensite and ferrite was approximately 15 mV for the DP WSs (as shown in Figs. 4 and 5). The above results can be explained as follows. In the initial stage of corrosion, the galvanic couple formed between the ferrite and pearlite was weaker than that formed between the martensite and ferrite. Thus, the WS treated with a normalizing heat treatment showed better electrochemical behavior than that treated with an intercritical annealing temperature of 820 °C. It has been shown that galvanic couples exist in normalized steel, and ferrite dissolves as an anode. Because pearlite is a mixture of ferrite and cementite lamellae, it is relatively inhomogeneous with respect to composition and structure. In DP WSs, the galvanic couple caused by the potential difference between the martensite and ferrite also exists (as

shown in Figs. 4 and 5). The low carbon content (0.06% C) and 3% Ni in the steel and marginal difference in the crystal structure between the ferrite and martensite resulted in a lower potential difference [4]. Considering the change in the ratio of the cathode area to the anode area and the potential between different structures, the galvanic couple may change with the corrosion process. For pearlite-ferrite normalized steel, the carbon enrichment at the grain boundaries acts as the cathode phase, enhancing the galvanic couple to accelerate ferrite corrosion (as can be seen in Fig. 10a from the surface morphology of the WS after the immersion experiment). This can explain why normalized steel had a higher corrosion rate in the long-term immersion experiment than that of the DP WS with an annealing temperature of 820 °C.

The relationship between corrosion behavior and heat treatment conditions is also discussed. When the annealing temperature was lower (820 °C), the average lath spacing was the smallest (250 nm) because the low temperature hindered the growth of the martensite laths. In addition,

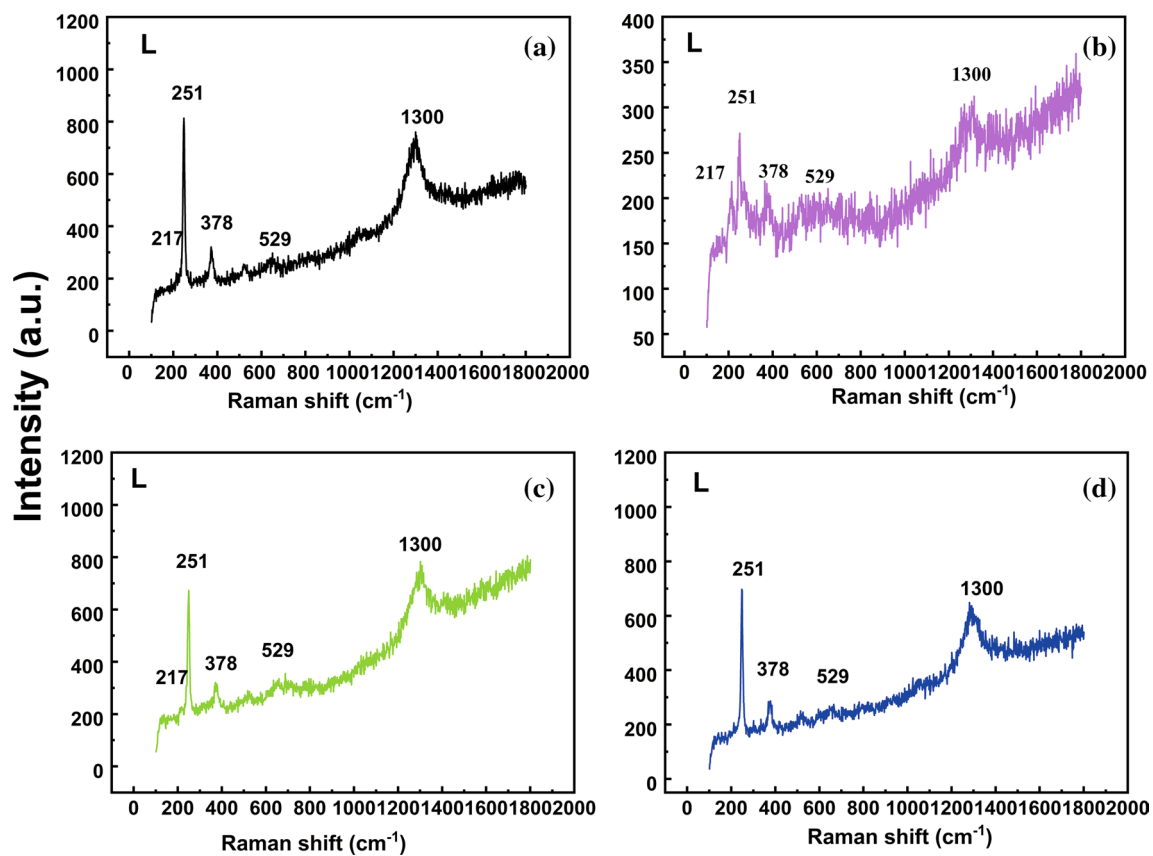


**Fig. 10** Raman results of the WSs after immersion for 30 d in a 3.5% NaCl solution: **a** none martensite, **b** 59.02% martensite, **c** 74.11% martensite, **d** 100% martensite

the ferrite had a lower dislocation density. In this case, the potentiodynamic polarization curve showed a positive displacement.

However, when the annealing temperature increased, the lath spacing of the martensite increased to 450 nm, and the dislocation density in the ferrite increased as well. The corrosion rates of the DP steels increased with increasing MVF. The AFM results (Fig. 5) show that the martensite potential in DP steel is positive, similar to the cathode phase. Increasing the MVF in the steel will enhance the unfavorable ratio of the cathode area to the anode area in the steel and increase the galvanic corrosion between the structures, thus increasing the corrosion rate. The corrosion resistance of DP steel was compared in this study as well as the studies by Bhagavathi and Sarkar, as mentioned in the introduction. Bhagavathi et al. [4] performed similar work and found that the corrosion resistance of DP steel is better than that of ferrite–pearlite steel. In their work, the variation in corrosion resistance with MVF was not significant for MVFs ranging from 21 to 28%. There are some differences between those studies and the experimental results presented here. First, in the study of Bhagavathi, the MVF of the DP steel was up to 28% lower than that of the 50.92% martensite samples in this

experiment. In the present work, the corrosion resistance of DP820 (50.92% MVF) is better than annealing steel, which is consistent with the results. This indicates that increasing the MVF in DP steel can reduce the corrosion rate. Sarkar et al. [22] reported that the island-like morphology of martensite provided better corrosion resistance compared to the network form surrounding the ferrite grains. In the present study, the martensite phase has a similar network-form morphology in the ferrite matrix. However, the microstructure of the martensite is fine, and the smallest average lath spacing was 250 nm because the low temperature hindered the growth of the martensite laths; thus, the DP steel exhibited better corrosion resistance. It is noteworthy that it is difficult to determine a specific numerical value. On the one hand, the differences in the elements in the steel and the structures obtained by different heat treatment processes are considerably different. Zhang et al. [19] used a traditional WS (09CuPCrNi). The steel used by Park et al. [29] was composed of 0.07% C, 0.83% Si, and 1.51% Mn. In the present work, Ni-advanced WS was adopted with 0.059% C, 0.087% Si, 1.23% Mn, and 3.21% Ni. On the other hand, it is difficult to quantitatively determine the size of galvanic corrosion because it is difficult to quantitatively measure the

unfavorable ratio of the cathode area to the anode area and the potential difference between the structures. Zhang et al. [34] reported a new simplified model to turn the galvanic corrosion problem of a complicated nonuniform system into a one-dimensional mathematical equation. They explained the influence of an increase in the SiCp volume fraction through mathematical calculation of the microgalvanic current density. This provides a new method for determining the microgalvanic corrosion caused by the martensite in DP steels. Galvanic corrosion caused by inclusions is very serious. However, the magnitude of various influencing factors can be quantitatively analyzed to help determine the difference in the corrosion resistance of steels. Therefore, a DP heat treatment can be used to obtain steel with better mechanical properties and corrosion resistance.

## 4 Conclusions

Dual-phase weathering steels with different MVFs were obtained by heat treatment. The corrosion behavior of the resulting steels was investigated using TEM, AFM, SEM, and electrochemical tests. The conclusions are as follows:

1. For four WSs, a galvanic couple forms between different parts of the microstructure, which leads to different corrosion morphologies on the surface of steel.
2. The microstructure of the DP WSs primarily consisted of martensite distributed in a ferrite matrix. With increasing MVF, the hardness of the DP WSs increased.
3. With increasing MVF in the DP WSs, the corrosion rate increased owing to the greater galvanic couple formed between the ferrite and martensite from the increasing ratio of the cathode area to the anode area. The high dislocation density in the martensite also affected the corrosion behavior.
4. Long-term immersion tests revealed that, while the morphology of the four WSs was different, the corrosion products were mainly composed of lepidocrocite.

**Acknowledgements** This work was financially supported by the National Key Research and Development Program of China (No. 2016YFB0300604) and the National Natural Science Foundation of China (No. 51671028).

## References

- [1] X.G. Li, D.W. Zhang, Z.Y. Liu, C.W. Du, C.F. Dong, *Nature* **1**, 441 (2015)

- [2] W. Wu, X.Q. Cheng, H.X. Hou, B. Liu, X.G. Li, *Appl. Surf. Sci.* **436**, 80 (2018)
- [3] X.Q. Cheng, Y.W. Tian, X.G. Li, C. Zhou, *Mater. Corros.* **65**, 1033 (2014)
- [4] L. Bhagavathi, G. Chaudhari, S. Nath, *Mater. Des.* **32**, 433 (2011)
- [5] X.Q. Cheng, Z. Jin, M. Liu, X.G. Li, *Corros. Sci.* **115**, 135 (2017)
- [6] T. Kamimura, S. Hara, H. Miyuki, M. Yamashita, H. Uchida, *Corros. Sci.* **48**, 2799 (2006)
- [7] X.L. Gao, G.Q. Fu, M.Y. Zhu, *Acta Metall. Sin. (Engl. Lett.)* **25**, 295 (2012)
- [8] X.H. Chen, J.H. Dong, E.H. Han, W. Ke, *Mater. Lett.* **61**, 4050 (2007)
- [9] M. Kimura, T. Suzuki, G. Shigesato, H. Kihira, S. Suzuki, *ISIJ Int.* **42**, 1534 (2002)
- [10] X.H. Chen, J.H. Dong, E.H. Han, W. Ke, *Can. Metall. Quart.* **46**, 195 (2007)
- [11] B. Mintz, *Int. Mater. Rev.* **46**, 169 (2001)
- [12] O. Keleştemur, S. Yıldız, *Constr. Build. Mater.* **23**, 78 (2009)
- [13] H.F. Lan, X.H. Liu, L.X. Du, *Acta Metall. Sin. (Engl. Lett.)* **25**, 443 (2012)
- [14] T. Hsu, Z. Xu, *Mater. Sci. Forum* **561–565**, 2283 (2007)
- [15] H. Hofmann, D. Mattissen, T.W. Schaumann, *Steel Res. Int.* **37**, 715 (2006)
- [16] O. Bouaziz, H. Zurob, M. Huang, *Steel Res. Int.* **84**, 937 (2013)
- [17] C.W. Zheng, D. Raabe, *Acta Mater.* **61**, 5504 (2013)
- [18] S. Kuang, Y.L. Kang, H. Yu, R.D. Liu, *Int. J. Miner. Metall. Mater.* **16**, 159 (2009)
- [19] C.L. Zhang, D.Y. Cai, B. Liao, T.Z. Zhao, Y.C. Fan, *Mater. Lett.* **58**, 1524 (2004)
- [20] T. Allam, M. Abbas, *Steel Res. Int.* **86**, 231 (2015)
- [21] Z.G. Liu, X.H. Gao, L.X. Du, J.P. Li, Y. Kuang, B. Wu, *Appl. Surf. Sci.* **351**, 610 (2015)
- [22] P. Sarkar, P. Kumar, M. Manna, P. Chakraborti, *Mater. Lett.* **59**, 2488 (2005)
- [23] A. Davoodi, J. Pan, C. Leygraf, S. Norgren, *Electrochim. Acta* **52**, 7697 (2007)
- [24] P.G. Ulyanov, D.Y. Usachov, A.V. Fedorov, *Appl. Surf. Sci.* **267**, 216 (2013)
- [25] C. Liu, R. Revilla, Z.Y. Liu, D.W. Zhang, X.G. Li, H. Terryn, *Corros. Sci.* **129**, 82 (2017)
- [26] J. Wei, J.H. Dong, W. Ke, X.Y. He, *Corros. Sci. Sec.* **21**, 1467 (2015)
- [27] C. Liu, R. Revilla, D.W. Zhang, Z.Y. Liu, A. Lutz, F. Zhang, T.L. Zhao, H.C. Ma, X.G. Li, H. Terryn, *Corros. Sci.* **138**, 96 (2018)
- [28] L. Cheng, Q.W. Cai, J.L. Lv, W. Yu, H. Miura, *J. Alloy. Compd.* **746**, 482 (2018)
- [29] K.S. Park, K.T. Park, D.L. Lee, C.S. Lee, *Mater. Sci. Eng. A.* **449–451**, 1135 (2007)
- [30] Q.F. Xu, K.W. Gao, Y.B. Wang, X.L. Pang, *Appl. Surf. Sci.* **345**, 10 (2015)
- [31] Y.G. Yang, T. Zhang, Y.W. Shao, G.Z. Meng, F.H. Wang, *Corros. Sci.* **71**, 62 (2013)
- [32] Z.Y. Cui, X.G. Li, C. Man, K. Xiao, C.F. Dong, X. Wang, Z.Y. Liu, *J. Mater. Eng. Perform.* **24**, 2885 (2015)
- [33] C. Thee, L. Hao, J.H. Dong, X. Mu, W. Ke, *Acta Metall. Sin. (Engl. Lett.)* **28**, 261 (2015)
- [34] C.Y. Zhang, T. Zhang, Y.Q. Wang, F.F. Wei, Y.W. Shao, G.Z. Meng, F.H. Wang, K. Wu, *J. Electrochem. Soc.* **162**, 754 (2015)